The relative merits of the S–B and conventional diffractometers may be evaluated as follows. The S–B has approximately five times higher intensity, the flat specimen aberration is eliminated for all diffraction angles by a single curvature, the stationary specimen simplifies the design and use of devices for varying the environmental conditions, and several detectors may be used simultaneously for dynamic studies or for reducing the scanning time. The disadvantages inherent in the geometry are: the angular range is limited and for the instrument used (Parrish, Mack & Vajda, 1967) the d-range is only 3·87 Å to 0·95 Å with Cu $K\alpha$ radiation, the inaccessible zero angle makes it necessary to use standard substances for angular calibration, extreme care must be used in specimen preparation to avoid intensity errors arising from surface roughness and large displacement errors at small diffraction angles, rotating flat specimens to reduce the effect of crystallite size statistics can be used only with small angular apertures thus reducing the intensity gain, the variation in the angular resolution in the variable ε^* S–B requires correction of the relative intensities. The conventional diffractometer is thus a more versatile and accurate general purpose instrument while the S–B should be utilized for certain special applications.

We are indebted to Mrs P. Harnack for technical assistance and Miss H. P. Goodman and Mrs M. L. Bonney for preparing the illustrations.

References

BAUN, W. L. & RENTON, J. J. (1963). *J. Sci. Instrum.* **40**, 498.
DAS GUPTA, K., SCHNOPPER, H. W., METZGER, A. E. & SHIELDS, A. R. (1966). *Advanc. X-ray Anal.* **9**, 221.
DUNNE, J. A. (1965). Techn. Memo. 33-218, p. 129, Jet Propulsion Lab., Pasadena, Calif., 1 June.
KUNZE, G. (1964). *Z. angew. Phys.* **17**, 412; **17**, 522; **18**, 28.
LEVY, H. A., AGRON, P. A. & DANFORD, M. D. (1959). *J. Appl. Phys.* **30**, 2012.
MILBERG, M. E. (1958). *J. Appl. Phys.* **29**, 64.
PARRISH, W. (1965). *X-ray Analysis Papers*. Eindhoven: Centrex Publishing Co.
PARRISH, W. & MACK, M. (1967). *Acta Cryst.* **23**, 687.
PARRISH, W., MACK, M. & VAJDA, I. (1967). *Norelco Reporter*, **14**, 56.
SEGMÜLLER, A. (1957). *Z. Metallk.* **48**, 448.
SEGMÜLLER, A. & WINCIERZ, P. (1959). *Arch. Eisenh.* **30**, 577.
WILSON, A. J. C. (1963). *Mathematical Theory of X-ray Powder Diffractometry*. Eindhoven: Philips Technical Library.

Acta Cryst. (1967). **23**, 700

The Atomic Radial Distribution Function in Amorphous Selenium

BY ROGER CHANG AND PAUL ROMO

North American Aviation Science Center, Thousand Oaks, California, U.S.A.

(*Received* 12 *April* 1967)

The atomic radial distribution curves for vitreous selenium quenched from two melt temperatures, 700 and 775 °K, were evaluated from X-ray diffraction measurements using Cu K and Mo K radiations and balanced filters. The general features of the radial density function are similar to those published in the literature. A consideration of the fine details of the radial density function suggests that quenching from different melt temperatures yields vitreous selenium of slightly different packings of the atoms at larger radial distances than the nearest neighbor separation of 2·3 Å. A quantitative correlation between the radial density function and the actual intermolecular structure of the material must await, however, better low-angle intensity data and accurate extension of the intensity curve to larger S values than used in this study.

Introduction

Earlier studies of the atomic radial distribution function in amorphous selenium have been reported by Richter and other investigators using X-ray diffraction (Richter & Herre, 1958; Lark-Horovitz & Miller, 1937; Hendus, 1942). More recently Henninger, Buschert & Heaton (1967) reinvestigated the problem with both X-ray and neutron diffraction. Henninger and coworkers concluded that the intensity function can largely be accounted for by considering only two interatomic distances between the first and second nearest neighbors along the c-axis chain structure of hexagonal crystalline selenium and that the spiral structure persists in the amorphous state with nearly unchanged geometry out to the second nearest neighbors but in random orientations.

The elastic and anelastic properties (in the megacycle frequency range), viscosity, and electrical resistivity of vitreous selenium near its glass transition temperature were measured as a function of the quench (or melt) temperature by Graham & Chang (1965). The meas-

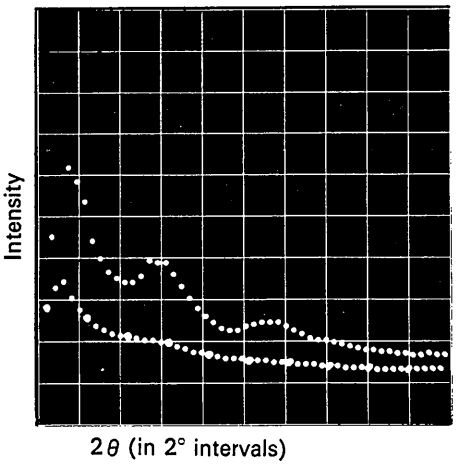

Fig. 1. Oscilloscope plot of counting rates, Mo K radiation (upper curve: Zr filter; lower curve: Y filter). Specimen no. 1 (775 °K quench).

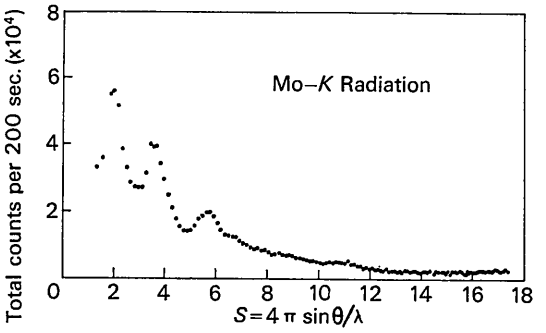

Fig. 2. Intensity *versus* $S=4\pi \sin\theta/\lambda$ of data converted from output shown in Fig. 1.

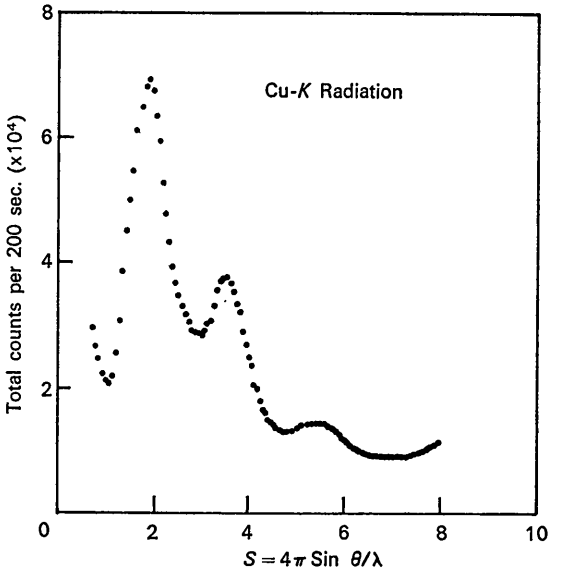

Fig. 3. Same as Fig. 2. Cu K Radiation.

urements reveal a correlation between the various properties and the intermolecular structure of the material at the quench temperature. It is the purpose of the present investigation to determine independently by means of X-ray diffraction whether there is a difference in the atomic radial distribution function of vitreous selenium prepared by quenching from different melt temperatures.

Theory

The atomic radial distribution function in a monatomic amorphous solid can be determined from X-ray diffraction data by means of the following formula (Zernicke & Prins, 1927):

$$T(r)=4\pi r^2[\varrho(r)=\varrho_0]=\frac{2r}{\pi}\int_0^\infty S\,.\,I(S)\,.\,\sin(rS)\,.\,dS\,, \tag{1}$$

where $\varrho(r)$ is the atomic density in atoms per unit volume at a radial distance r from a given atom, assumed to be spherically symmetric in the time average over all possible atomic configurations; ϱ_0 is the macroscopic average atomic density; $S=4\pi \sin\theta/\lambda$, θ being the angle of incidence and λ the wave length of the X-ray beam; and $I(S)$ is the following experimental intensity function:

$$I(S)=\left[\frac{I_0(S)\,.\,K-I_c(S)}{F^2(S)}\right]-1\,, \tag{2}$$

where $I_0(S)$ is the total measured diffracted intensity at angle 2θ corrected for background, polarization, and absorption effects; K is a normalization constant converting the experimental intensity to electron units per atom; $I_c(S)$ is the theoretical Compton modified scattering per atom; and $F(S)$ is the theoretical atomic scattering factor after anomalous dispersion corrections.

Experimental

A General Electric model XRD-5 diffractometer and associated detecting equipment were used to determine the X-ray diffracted intensities. Effective monochromatization of the X-ray beam was achieved by use of the appropriate filter and pulse-height analyzer combination. Both Cu K radiation with Ni–Co balanced filters and Mo K radiation with Zr–Y balanced filters were used. Each filter was balanced at the $K\beta$ peak to less than one per cent for each radiation before each run. The conventional counter-spectrometer technique using reflected beam and parafocusing geometry, where the counter moves twice the angle of rotation of the specimen, was used. Fluorescence background was minimized by using aluminum foils of appropriate thicknesses. Total counts at a given 2θ were obtained at one degree intervals for a time interval of 200 seconds, using scintillation counting techniques. The entire apparatus was automated and programmed to record the count data on punched tape for 2θ values from 10 to 160°, covering S values from 0·7 to 17·4. The punched data were fed directly to an IBM 360 computer to

yield the atomic radial distribution curves. The program includes procedures to fit together the Cu and Mo data. Details of the instrumentation will be described in a separate publication.*

Selenium of 99·999% purity was sealed in thin-walled glass tubing at a pressure of 10^{-5} torr, maintained at the desired temperature for 3–4 hours, then quenched in silicone oil to room temperature. The quenched material was then vacuum pressed at a pressure of about 10^{-5} torr between mirror-polished steel plattens (load 100 kg, temperature 56 °C, time 30 min) into samples of approximately 2·5 cm in diameter and 0·25 cm thick for X-ray diffraction measurements. This procedure was chosen in order to duplicate that used in the previous work by Graham & Chang (1965). Two quench temperatures, 700 and 775 °K, were used, since significant difference in the intermolecular structure of vitreous selenium is expected for the two quench temperatures. Duplicate runs were made for each quench temperature, starting from the very beginning of specimen preparation.

Analyses of data

A typical oscilloscope plot of the counting data for specimen no. 1 (775 °K quench, Mo K radiation, Zr–Y filter) is reproduced in Fig. 1, where the upper and lower traces are the counting data for the Zr and Y filters respectively (this particular plot was made for 2θ at 2° intervals). The difference in counts for the two filters at each 2θ angle is obtained at 1° intervals and plotted *versus* the S values in Fig. 2. A similar plot for the same specimen using Cu K radiation and a Ni–Co filter pair is shown in Fig. 3. The observed intensities shown in Figs. 2 and 3 were combined and converted to absolute electron units per atom by using the appropriate normalizing constant K for each radiation at large S values to satisfy the following:

$$I_o(S) \cdot K - I_c(S) = F^2(S) , \qquad (3)$$

where the various parameters appearing in equation (3) are defined as before. In the actual Fourier transformation of the intensity data to yield the atomic radial distribution function, the Cu K data between $S=0·7$ and $S=4·8$ and the Mo K data between $S=4·8$ and $S=17·4$ are used since it is believed that the low angle data for the Cu K radiation are more precise than those obtained with the Mo K radiation.

Since we are interested in detecting small differences in the radial density function of selenium specimens quenched from slightly different melt temperatures (700 *versus* 775 °K), it is thought not advisable to use the smoothing procedures recently developed by Kaplow, Strong & Averbach (1965). Instead, an arbitrary damping factor $\exp[B(4\pi \sin\theta/\lambda)^2]$, with B varying from

* In collaboration with W. V. Johnston.

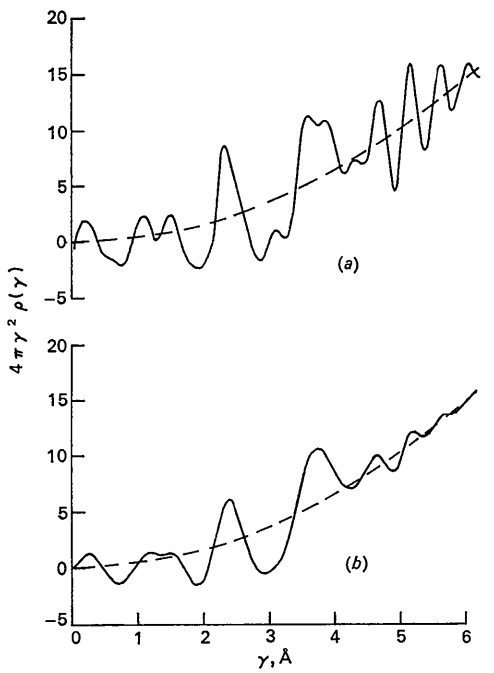

Fig. 4. Atomic radial distribution curves, specimen no. 3 (700 °K quench) obtained with two damping constants, (*a*) $B=-0·01$ and (*b*) $B=-0·02$.

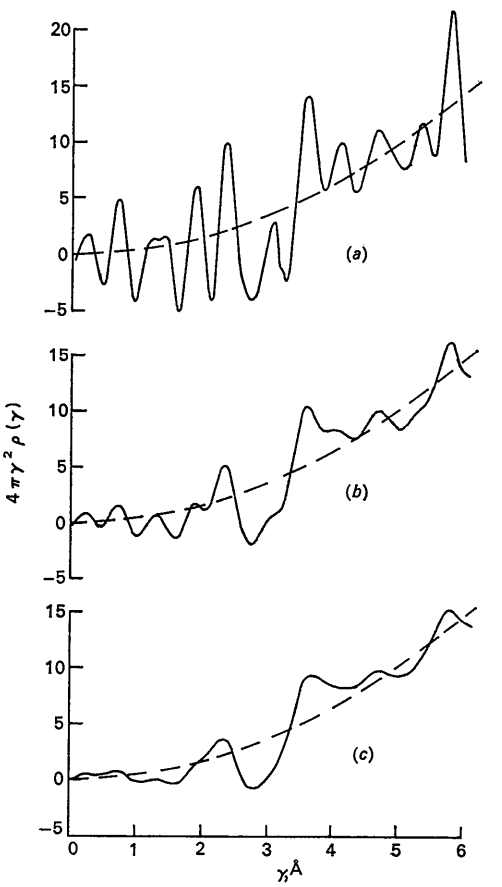

Fig. 5. Atomic radial distribution curves, specimen no. 2 (775 °K quench) obtained with three damping constants, (*a*) $B=0$, (*b*) $B=-0·01$ and (*c*) $B=-0·02$.

zero to any negative number in small steps, was applied to the experimentally observed intensity to yield a series of variously damped radial distribution curves for subsequent examination. This procedure is considered necessary since details of the radial density function will become increasingly more obscure with higher damping (more negative damping constant B). For example, the radial distribution curve obtained by Henninger *et al.* (1967) (Fig. 6 of their paper) is believed to be highly damped as the half-width of the 2·3 Å peak is nearly 0·4 Å while the same peak from our less severely damped curves exhibits a half-width of about 0·15 to 0·20 Å.

Fig. 4 shows the atomic radial distribution curves for specimen no. 3 (700°K quench) obtained with two damping constants $B=-0{\cdot}01$ and $B=-0{\cdot}02$. Except for the spurious peaks at r values less than 2·3 Å (the nearest neighbor distance), principal peaks are noted at 2·3 and 3·7 Å, and less prominent peaks at 4·7, 5·2 and 5·6 Å [Fig. 4(*b*), $B=-0{\cdot}02$]. However, the same radial distribution curve obtained with a smaller damping constant (Fig. 4(*a*), $B=-0{\cdot}01$) shows the existence of two additional small peaks* at 3·1 and 4·3 Å and suggests that the 3·7 Å peak may actually be composed of two separate peaks at 3·6 and 3·9 Å. The two radial distribution curves ($B=-0{\cdot}02$) obtained by truncation to $S_{max}=10{\cdot}4$ and 14·1 almost coincide with that shown in Fig. 4(*b*).

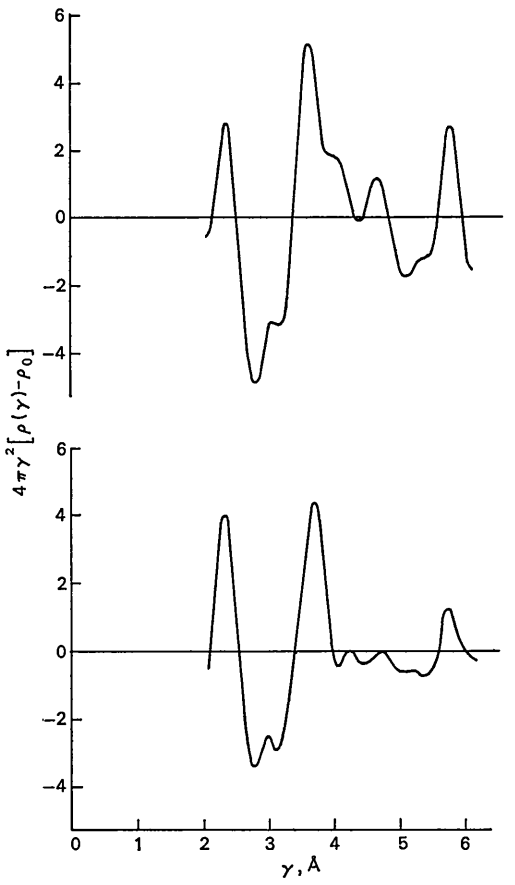

Fig. 6. Comparison of radial density function of this work (upper curve, specimen no. 1, 775°K quench) and the work of Henninger *et al.* (lower curve, reproduced from Fig. 8 of Henninger, Buschert & Heaton, 1967).

The atomic radial distribution curves for specimen no. 2 (775°K quench) obtained with three damping constants, $B=0$, $-0{\cdot}01$ and $-0{\cdot}02$, are shown in Fig. 5(*a*), (*b*), and (*c*) respectively. Distinct peaks are observed at 2·3, 3·6, 4·1, 4·7, 5·3, and 5·8 Å. The resolution for the artifically damped curve (Fig. 5(*c*), $B=-0{\cdot}02$) was so poor that details of the 4·1 and 5·3 Å peaks were nearly lost. The presence of a small peak at 3·1 Å is also visible in Fig. 5(*a*) and (*b*).

A comparison of the atomic radial distribution curves for the two quench temperatures shows the following:

(1) The principal peak at 2·3 Å is nearly identical for the two quench temperatures, the area under the peak being about 2·0 for the 700°K quench and 2·1 for the 775°K quench.

(2) The 3·7 Å peak for the 700°K quench appears to be composed of two separate peaks at 3·6 Å and 3·9 Å.

(3) The 5·3 Å peak for the 775°K quench is shifted to about 5·2 Å for the 700°K quench.

(4) The 5·8 Å peak for the 775°K quench is replaced by a peak of considerably lower intensity at 5·6 Å and possibly a second one at 6·1 Å.

(5) The results are reproducible for the duplicate specimens quenched from each temperature.

Discussion

The principal features of the radial density function reported here agree in general with those reported by Richter & Herre (1958), Lark-Horovitz & Miller (1937) and Hendus (1947) and by Henninger, Buschert & Heaton (1967). A typical comparison is shown graphically in Fig. 6. However, there are definite differences between this work and that of Henninger *et al.* with regard to the position and intensity of the less prominent peaks. We believe that our observations are real, although the quantitative nature of these less prominent peaks may be somewhat modified by further corrective and smoothing procedures. First, these peaks are located at relatively large values of r and are not appreciably affected by these corrective and smoothing procedures. Second, our specimens were prepared by vacuum warming pressing of selenium quenched from the melt temperature while Henninger used evaporated thin films. It is therefore our first conclusion that quenching from different melt temperatures produces amorphous selenium of varying intermolecular structure as evidenced by small differences in the atomic radial distribution curves.

* They could be, although it is unlikely, ripples associated with the 3·7 Å peak.

Graham & Chang (1965) have speculated from thermodynamic considerations that vitreous selenium quenched from 775°K has smaller average molecular weight than that quenched from 700°K. The results of this study suggest that quenching from different melt temperatures does not seem to affect significantly the nearest neighbor packing but may affect the configurational arrangement of atoms at larger radial distances. It is not believed possible at this stage, however, to relate the small differences in the radial density function from X-ray diffraction studies to the intermolecular structures in any quantitative way, although Richter & Herre (1958) have approached the problem by assuming the presence of layered structures to account for the presence of additional peaks in the radial density function. In order to attack the problem on a more quantitative basis, it is essential to improve further the accuracy of experimental data acquisition and to extend such data collection to lower as well as larger S values than those reached in this work.

The authors wish to thank Stephen T. Imrich, North American Aviation Science Center, for help on data reduction and programming details.

References

GRAHAM, L. J. & CHANG, R. (1965). *J. Appl. Phys.* **36**, 2983.
HENDUS, H. (1942). *Z. Physik*, **119**, 265.
HENNINGER, E. H., BUSCHERT, R. C. & HEATON, L. (1967). *J. Chem. Phys.* **46**, 586.
KAPLOW, R., STRONG, S. L. & AVERBACH, B. L. (1965). *Phys. Rev.* **138**, A1336.
LARK-HOROVITZ, K. & MILLER, E. P. (1937). *Phys. Rev.* **51**, 380.
RICHTER, H. & HERRE, F. (1958). *Z. Naturforsch.* **13** A, 874.
ZERNICKE, F. & PRINS, J. A. (1927). *Z. Physik*, **41**, 184.

Acta Cryst. (1967). **23**, 704

Study of Chrysotile Asbestos by a High Resolution Electron Microscope

BY KEIJI YADA

Research Institute for Scientific Measurements, Tohoku University, Sendai, Japan

(*Received* 22 *May* 1967 *and in revised form* 19 *July* 1967)

Microfibers of chrysotile asbestos were observed from two directions parallel and perpendicular to the fiber axis by selected area electron diffraction and high resolution electron microscopy. The results are as follows: (*a*) Most of the fibers have a hollow cylindrical form. Some fibers, however, are not hollow but solid, showing an unusual growth pattern. (*b*) Splitting of diffraction spots is observed with a highly parallel illumination. (*c*) The observed dislocation patterns suggest that the value of the c parameter is 7·3 Å rather than 14·6 Å. (*d*) The lattice image observed in the cross sections of fiber shows multi-spiral lattice fringes instead of concentric ones, in conformity with the hypothesis of Jagodzinski and Kunze.

Introduction

Since the first work by Warren & Bragg (1930), the crystal structures of chrysotile asbestos have been studied by many workers not only by X-ray diffraction but also by electron microscopy and electron diffraction (Warren & Herring, 1941; Aruja, 1943; Padurow, 1950; Bates, Hildebrand & Swineford, 1950; Whittaker, 1951; Brindley, 1952; Honjo & Mihama, 1954; Jagodzinski & Kunze, 1954*a*,*b*,*c*; Whittaker, 1954, 1955, 1956; Whittaker & Zussman, 1956; Zussman, Brindley & Comer, 1957). However, more detailed studies seem to be necessary concerning the form of microfibers, lattice parameters, and crystal growth mechanism.

The resolution of electron microscopes has been so markedly improved that nowadays it is possible to observe the lattice planes, as lattice fringes, of spacings in the 1·5–2 Å range when the crystalline specimens satisfy Bragg conditions appropriately and their thicknesses are suitable. The tilted illumination method had been recommended for such high resolution work (Dowell, 1963; Komoda, 1966). Recently, however, it has been shown that lattice resolution attained by the axial illumination method can be as high as that obtained with tilted illumination (Yada & Hibi, 1966), and, as a result, it becomes very easy to obtain the lattice images of isolated small specimens such as chrysotile fibers.

Fernández-Morán (1966) observed the lattice images on chrysotile fibers which were used as supporters of micro-organisms, and utilized the lattice fringes for the calibration of magnification. In the present work, microfibers of chrysotile were observed by means of a high resolution electron microscope in order to study the crystal structure and the crystal growth mechanism.

Specimen and experimental

The specimen used in the present work was micropulverized chrysotile from Jeffrey mine, Canada. Ac-